Available online at www.sciencedirect.com
ScienceDirect
Journal of Sound and Vibration 322 (2009) 438–453
JOURNAL OF SOUND AND VIBRATION
www.elsevier.com/locate/jsvi

Dynamic system change detection using a modification of the transfer entropy

L.A. Overbey, M.D. Todd*

Department of Structural Engineering, University of California, San Diego, La Jolla, CA 92093-0085, USA

Received 27 October 2007; received in revised form 28 October 2008; accepted 7 November 2008
Handling Editor: S. Bolton
Available online 30 December 2008

Abstract

Recent work has validated the use of transfer entropy for exploring coupling in structural dynamics. Transfer entropy is a measure of information flow between Markov processes. Using transitional probabilities, one can get a quantification of the degree of influence one process has on the dynamics of another. Previous research included a time lag to assess information exchanges at various time scales without resulting in tremendously burdensome computations. However, it is more informative to view the transfer entropy using two separate time lags to assess transitional probabilities between both processes. This work introduces a second time delay into a linearized version of the transfer entropy to produce a transfer entropy surface. This surface allows for a fuller assessment of dynamical coupling between measurements. Analytical and low-order-correlation-based measures of the transfer entropy were formed and compared to common modal analysis methods to assess their ability to detect linear dynamical changes in structures. Investigations were conducted on a computational linear oscillator and a simple experimental system. The transfer entropy is a much better indicator of dynamical changes than the modal techniques. For the structural systems studied, the plane of greatest sensitivity in the time-delayed transfer entropy surface is along the diagonal and not along one coordinate as was utilized in previous work.

1. Introduction

There are a great number of system identification procedures that rely on examining linear dynamical relationships between data. The underlying assumption in these procedures is that a system may be decomposed into its eigenstructure, resulting in orthogonal normal modes vibrating at their corresponding eigenfreqencies. The procedure commonly involves recording system inputs and outputs, and then fitting the data to a linear model in the time or frequency domains. Common methods involve curve fitting frequency response functions, including the use of operating shapes (“peak picking”), rational polynomial curve fitting [1], and nonlinear least-squares fitting [2]. Additionally, there are several time domain approaches such as the eigensystem realization algorithm [3] and the complex exponential algorithm [4] among others [5,6]. Higher-order frequency response functions have been employed with some success to account for weak nonlinearities

*Corresponding author. Tel.: +1 858 5345951; fax: +1 858 5346373.
E-mail address: mdt@ucsd.edu (M.D. Todd).

0022-460X/$ - see front matter © 2008 Elsevier Ltd. All rights reserved.
doi:10.1016/j.jsv.2008.11.025

in systems [7,8]. This approach allows for nonlinear behavior but still requires model-based assumptions about the correlations within the system.

Recently, a generalized information-based approach was proposed utilizing the transfer entropy [9–11]. This approach examines structural dynamics from the perspective of information transfer between locations on a structure. Information theory was originally derived for the purposes of finding fundamental limits on compressing and reliably communicating data. Measures of information typically express uncertainties in random variables or in the relationship between random variables, and include the information entropy, mutual information, Kullback–Leibler divergence, and transfer entropy [12]. Transfer entropy specifically utilizes conditional relationships between two processes to determine degree and direction of information flow. For example, given two observations $x(n)$ and $y(n)$, the transfer entropy $T_{y\to x}$ measures the influence $y(n)$ has on the transition from $x(n)$ to $x(n+1)$. Previous works introduced a time delay τ into the algorithm to examine the influence of y on x at multiple time scales such that $y(n)$ becomes $y(n-\tau)$. While valid, this technique ignores the transitions from $x(n)$ to $x(n+1)$ at other time scales τ for the variable x, $x(n-\tau)$. This will be discussed at greater length in the following section, but the missing time scale influence is clear. Therefore, it would be more advisable to introduce time delays for both x and y. A transfer entropy *surface* can be thus created that explores the relationship between transitions at all these various time scales.

This paper introduces this variation to transfer entropy and examines how changes to system dynamics affect the transfer entropy at various time scales. Estimation of transfer entropy can be quite difficult, requiring a large number of points to reduce variance in results; however, for linear systems subject to Gaussian excitation, an analytical formula can be derived. The formula incorporates the use of a combination of time-delayed auto- and cross-correlations. Consequently, a data-based "linear" estimation [10] can be made through the estimation of these correlations. This linearized estimate of the transfer entropy can be employed similar to the previously mentioned modal analysis techniques for systems where linear assumptions hold true.

In this work, the linear modified transfer entropy for a simulated multi-degree-of-freedom oscillator is computed and validated through comparisons to theoretical results. In addition, techniques are evaluated for utilizing this modified transfer entropy as a low-dimensional indicator of a change to a dynamic system. It will be shown that certain time scales in the transfer entropy surface are more sensitive to damage than those time scales examined in previous works. The sensitivity of the linearized estimate of the transfer entropy is then compared to other time domain techniques as well as common frequency-based modal techniques for both the computational and experimental dynamic systems.

2. Time-delayed transfer entropy surface

Transfer entropy, originally formulated to examine information transport [9], explicitly accounts for the underlying dynamics between processes, unlike other information-based measures such as mutual information [13]. As stated previously, the formulation of transfer entropy involves the assessment of various conditional probabilities. If the dynamics of a process x at $x(n+1)$ is conditional only on previous values of x up to a time lag k, the process is called a kth-order Markov process. This transition probability can be written as $p(x(n+1)|x(n),x(n-1),\ldots,x(n-k+1)) = p(x(n+1)|x(n)^{(k)}) = p(x(1)|x^{(k)})$ (where n is dropped for notational convenience). If a second process $y(m)^{(l)}$ is influencing these transition probabilities, the influence of both $x(n)^{(k)}$ and $y(n)^{(l)}$ on $x(n+1)$ can be expressed as $p(x(1)|x^{(k)},y^{(l)})$. Based on the definition of dynamical interdependence, the transfer entropy [9] can be formulated as

$$T_{y\to x}(x(1)|x^{(k)},y^{(l)}) = \int\int\int p(x(1)|x^{(k)},y^{(l)}) \log_2\left(\frac{p(x(1)|x^{(k)},y^{(l)})}{p(x(1)|x^{(k)})}\right) \mathrm{d}x(1)\,\mathrm{d}x^{(k)}\,\mathrm{d}y^{(l)}. \tag{1}$$

Hence, transfer entropy provides a quantification of the additional knowledge provided by the observation y that is necessary to describe the future dynamics of x, given that the past history of x is already known. To compute this equation from data, one would be required to estimate very high-dimensional probability densities. Previous works that have employed transfer entropy in a structural dynamics application [10,11] have reduced the order of the processes to $k = l = 1$ for computational simplicity, and a time delay is added

to $y(n)$ such that the transfer entropy equation becomes

$$T_{y\to x}(x(1)|x,y(\tau)) = \int\int\int p(x(1)|x,y(\tau))\log_2\left(\frac{p(x(1)|x,y(\tau))}{p(x(1)|x)}\right)\mathrm{d}x(1)\,\mathrm{d}x\,\mathrm{d}y(\tau), \tag{2}$$

where $y(\tau)\equiv y(n+\tau)$. Assuming the process truly is of order $k=l=1$, this equation quantifies the information gain from $y(\tau)$ *only*. However, most structural systems do not easily fit into such a low-order process. Therefore, information about the dynamics of x may be present within its own past history, such that when $y=x$, Eq. (2) will not be zero. This equation can still provide useful information in regard to process couplings [10,11], but does not strictly adhere to a definition of transfer entropy that calls it *a measure of the information gain from y on the dynamics of x given that the past history of x has already been accounted for*. In systems that can be represented by a set of ordinary differential equations or a mapping, x and y can be represented by vectors, in which case the transfer entropy can account for the full dynamics with a low Markov order. However, the vector representation would still require the estimation of high-dimensional probability densities.

In order to include the full past history of x and y without requiring extremely high-dimensional probability density functions (pdfs), one can incorporate time lags into both $x(n)$ and $y(n)$ such that

$$T_{y\to x}(x|x(\tau_1),y(\tau_2)) = \int\int\int p(x|x(\tau_1),y(\tau_2))\log_2\left(\frac{p(x|x(\tau_1),y(\tau_2))}{p(x|x(\tau_1))}\right)\mathrm{d}x\,\mathrm{d}x(\tau_1)\,\mathrm{d}y(\tau_2), \tag{3}$$

where $x\equiv x(n)$, $x(\tau_1)\equiv x(n+\tau_1)$, and $y(\tau_2)\equiv y(n+\tau_2)$. Note that $x(1)$ in Eq. (2) was replaced with x in Eq. (3) because all delay combinations between the three variables are possible using the two lags τ_1 and τ_2. When $\tau_1=-1$ and $\tau_2=\tau$, Eq. (3) is equivalent to Eq. (2). Examining the surface created by a range of τ_1 and τ_2 values, one can obtain an assessment of the information transfer from y to the current dynamics of x at multiple simultaneous time scales of x and y. For any set of values τ_1 and τ_2, the transfer entropy measure in Eq. (3) will still have a bias caused by not taking into account the entire past history of x all at once. However, by viewing all values of τ_1 and τ_2 in this *transfer entropy surface*, one can intuitively see where the perceived additional influence of y at τ_2 could be attributed to the past history of x if a higher-order Markov process was considered. This can be better understood by examining an analytical solution to the transfer entropy surface, as will be derived below for linear Gaussian dynamical systems.

Expanding the conditional probabilities in Eq. (3), the transfer entropy can be rewritten in entropy form as

$$\begin{aligned} T_{y\to x}(x|x(\tau_1),y(\tau_2)) = {} & \int\int\int p(x,x(\tau_1),y(\tau_2))\times\log_2(p(x,x(\tau_1),y(\tau_2)))\,\mathrm{d}x\,\mathrm{d}x(\tau_1)\,\mathrm{d}y(\tau_2) \\ & + \int p(x)\times\log_2(p(x))\,\mathrm{d}x - \int\int p(x,y(\tau_2))\times\log_2(p(x,y(\tau_2)))\,\mathrm{d}x\,\mathrm{d}y(\tau_2) \\ & - \int\int p(x,x(\tau_1))\times\log_2(p(x,x(\tau_1)))\,\mathrm{d}x\,\mathrm{d}x(\tau_1). \end{aligned} \tag{4}$$

Assuming stationarity and ergodicity, the probabilities can be estimated from a single x and y time series. However, for linear Gaussian dynamical systems, analytical and linearized (defined here as estimations made when assuming no higher than second-order correlations in the data) formulations of the measure can be established to avoid estimation of multidimensional pdfs. For Gaussian processes, the transfer entropy can be written as the product of determinants of covariance matrices [14]. For the general, possibly multivariate case, the expression becomes

$$T_{y\to x}(x|x(\tau_1),y(\tau_2)) = \frac{1}{2}\log_2\left[\frac{|C_{x,x(\tau_1),y(\tau_2)}||C_x|}{|C_{x,y(\tau_2)}||C_{x,x(\tau_1)}|}\right], \tag{5}$$

where C_x, $C_{x\otimes x(\tau_1)}$, $C_{x\otimes y(\tau_2)}$, and $C_{x\otimes x(\tau_1)\otimes y(\tau_2)}$ represent the covariance matrices associated with x, $x\otimes x(\tau_1)$, $x\otimes y(\tau_2)$, and $x\otimes x(\tau_1)\otimes y(\tau_2)$, respectively. The operator $|\cdot|$ takes the determinant. The transfer entropy assuming a Gaussian-excited linear system can therefore be computed by taking the various expected values in Eq. (5). If x and y are stationary, ergodic, zero-mean processes, the time-shifted cross-correlation between them can be written as $R_{xy}(\tau_2-\tau_1)\equiv E[x(n+\tau_1),y(n+\tau_2)]$. For convenience, the autocorrelations can be normalized to $\rho_{xx}(\tau_1)\equiv R_{xx}(\tau_1)/R_{xx}(0)$ and $\rho_{yy}(\tau_1)\equiv R_{yy}(\tau_1)/R_{yy}(0)$, and the linear cross-correlation coefficient

can be expressed as $\rho_{xy}(\tau_2-\tau_1) \equiv R_{xy}(\tau_2-\tau_1)/\sqrt{R_{xx}(0)R_{yy}(0)}$. It can also be noted that $\rho_{xy}(\tau_2-\tau_1) = \rho_{yx}(\tau_1-\tau_2)$. Using this notation, Eq. (5) can be written as

$$T_{y\to x}(x|x(\tau_1),y(\tau_2)) = \frac{1}{2}\log_2\left[\frac{(\rho_{xx}^2(\tau_1)-1)(\rho_{xy}^2(\tau_2-\tau_1)-1)}{1+2\rho_{xx}(\tau_1)\rho_{xy}(\tau_2)\rho_{xy}(\tau_2-\tau_1)-\rho_{xy}^2(\tau_2)-\rho_{xx}^2(\tau_1)-\rho_{xy}^2(\tau_2-\tau_1)}\right]. \tag{6}$$

This equation forms the transfer entropy surface for a structure given that it is linear and Gaussian-excited. Eq. (6) incorporates both auto- and cross-correlations at various delays depending on the values of τ_1 and τ_2. If $\tau_1 = -1$, the equation becomes what has been used previously in the literature [10,11]. Ideally, the information gain through knowledge of y when the history of x is already known should be zero when $x = y$ and $\tau_2 \geqslant 0$. However, this will not be the case in the above expression for $x = y$ and $\tau_1 \neq \tau_2$, illustrating the bias attributed to low-order Markov assumptions. Therefore, assuming simultaneous measurements, only $\tau_1 = \tau_2 = \tau$ will not possess this bias. However, it may be useful in a dynamical examination to look at all variations of τ_1 and τ_2. If $\tau_1 = \tau_2 = \tau$, the equation reduces to a combination of auto and cross-correlations at τ and cross-correlations at zero. If $\tau_1 = \tau_2 = 0$, the transfer entropy becomes negative infinity, as no transition has taken place in this scenario.

The complete analytical solution for this type of system requires a solution to the auto- and cross-correlations in the above expression. The dynamics of an L-degree-of-freedom linear, dissipative, Gaussian-excited structure are typically written in the form:

$$\mathbf{M}\ddot{\mathbf{x}} + \mathbf{C}\dot{\mathbf{x}} + \mathbf{K}\mathbf{x} = \mathbf{f}(t), \tag{7}$$

where $\mathbf{M}$, $\mathbf{C}$, and $\mathbf{K}$ represent the L by L constant coefficient mass, damping, and stiffness matrices, respectively, and $f(t)$ is the Gaussian input. From [11], the linear cross-correlation between any two state variables in the above system is given by

$$R_{xy}(\tau) = \frac{1}{4}\sum_{l=1}^{L}\sum_{m=1}^{L} u_l(L)u_m(L)u_l(x)u_m(y)[A_{lm}\,\mathrm{e}^{-\varsigma_m\omega_m\tau}\cos(\omega_{dm}\tau) + B_{lm}\,\mathrm{e}^{-\varsigma_m\omega_m\tau}\sin(\omega_{dm}\tau)], \tag{8}$$

where u_i are the mode shapes and ω_i the undamped natural frequencies. Additionally, ς_i are the dimensionless damping ratios defining the fraction of critical (required for oscillatory behavior) in the ith mode, and ω_{di} are the corresponding damped natural frequencies such that $\omega_{di} = \omega_i\sqrt{1-\varsigma_i^2}$. Finally, the parameters A_{lm} and B_{lm} can be evaluated by

$$A_{lm} = \frac{8(\omega_l\varsigma_l + \omega_m\varsigma_m)}{\omega_l^4 + \omega_m^4 + 4\omega_l^3\omega_m\varsigma_l\varsigma_m + 2\omega_l^2\omega_m^2(-1+2\varsigma_l^2+2\varsigma_m^2)},$$

$$B_{lm} = \frac{4[\omega_l^2 + 2\omega_l\omega_m\varsigma_l\varsigma_m + \omega_m^2(-1+2\varsigma_m^2)]}{\omega_{dm}[\omega_l^4 + \omega_m^4 + 4\omega_l^3\omega_m\varsigma_l\varsigma_m + 2\omega_l^2\omega_m^2(-1+2\varsigma_l^2+2\varsigma_m^2)]}. \tag{9}$$

The purely analytical transfer entropy is useful for comparison to linearized (estimated from auto- and cross-correlations) and generalized estimates that do not assume the system is linear (by estimating the entropies in Eq. (4)). However for the scope of this work, results are limited to the analytical and linear estimate versions.

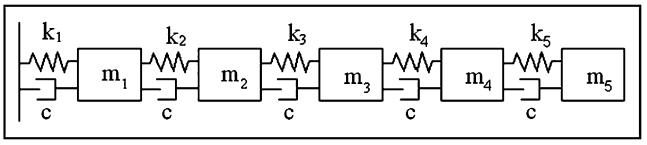

Fig. 1. Five-degrees-of-freedom linear spring mass model.

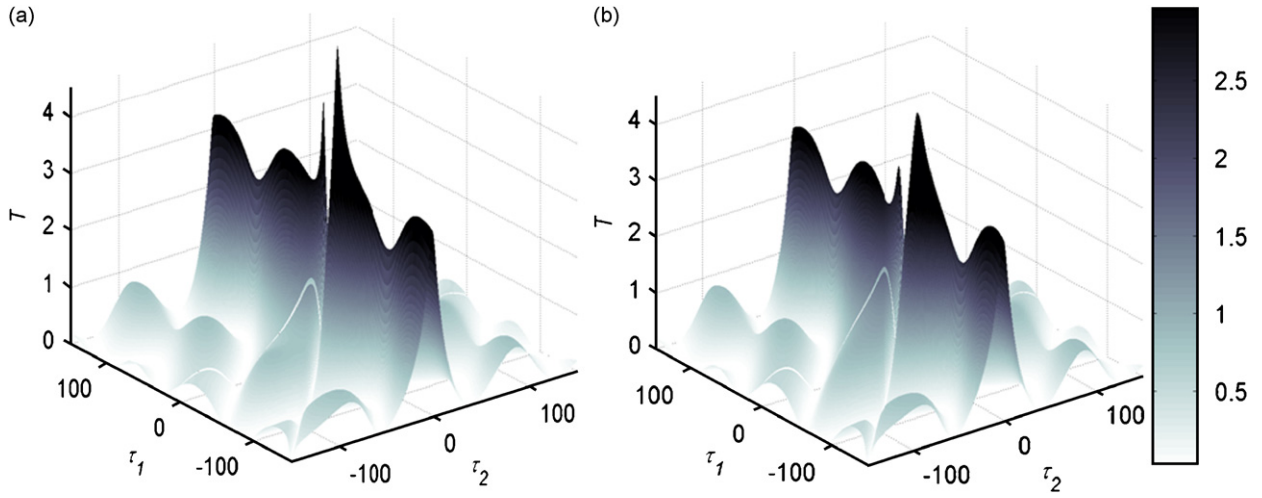

Fig. 2. Analytical transfer entropy surfaces for (a) $T_{x_3\to x_2}(\tau_1,\tau_2)$ and (b) $T_{x_4\to x_3}(\tau_1,\tau_2)$.

3. Simulated model

A simulated oscillator that can be described by Eq. (7) was constructed (Fig. 1) with baseline parameters set to $m_i = 0.002\,\text{kg}$, $c_i = 0.1\,\text{N s/m}$, and $k_i = 30\,\text{N/m}$. A random white Gaussian excitation was applied at the free end. The system was numerically integrated and discretely sampled at 1000 Hz.

Analytical transfer entropy surfaces are shown in Fig. 2 for a few different adjacent response comparisons in the baseline condition, spanning delay ranges of $-150\leqslant\tau_1\leqslant150$ and $-150\leqslant\tau_2\leqslant150$. When τ_1 is such that $x(n-\tau_1)$ is highly correlated with $x(n)$ ($\tau_1\approx\pm100$, corresponding to $f_s/2\omega_1$, where f_s is the sampling rate and ω_1 is the first natural frequency), the transition from $x(n-\tau_1)$ to $x(n)$ is fairly certain (higher conditional probability). Therefore, regardless of τ_2, the transfer entropy surface tends to approach a local minimum when these delays are reached in τ_1. Similarly, $y(n-\tau_2)$ provides additional knowledge about the transition from $x(n-\tau_1)$ to $x(n)$ when $x(n-\tau_1)$ is uncorrelated with $x(n)$, but $y(n-\tau_2)$ is strongly correlated with $x(n)$. For a linear system, this relationship will typically transpire near where $\tau_2-\tau_1$ is at a maximum or minimum in the cross-correlation function between x and y. Therefore, in the transfer entropy surface, there are diagonals of local minima where $\tau_2-\tau_1\approx\pm100$. Obviously, the local maxima in the transfer entropy appear between these local minima. Note that for many systems, including the system examined here, the autocorrelations of x and y are very similar to the cross-correlation between x and y when x and y are measured from adjacent locations. Therefore, the transfer entropies that exhibit minima and maxima along these $\tau_2-\tau_1$ diagonals do not truly express information gain from y given full knowledge of x because of the first-order assumption in the Markov model described previously. For higher-order Markov processes, the information transfer between y and x would actually be lower at these local maxima. This is the case because much of the information $y(n-\tau_2)$ adds to the transition from $x(n-\tau_1)$ to $x(n)$ is actually contained at another lag τ_1' that would have been accounted for at some higher order of the Markov expression for x. For an ideally ordered calculation, transfer entropy between a measurement and itself should be zero for any delay. Therefore, transfer entropies along the surface for this first-order approximation are skewed by what could be called a "false auto-transfer entropy," $T_{x\to x}(\tau_1,\tau_2)$. This is the transfer entropy bias described earlier. In addition, the flow of information can be further complicated by the difficulty in interpreting time scales of information transfer in the presence of bi-directional coupling.

Assuming simultaneous measurements, the only points along this surface that will not have a transfer entropy value between a measurement and itself are along the $\tau_1=\tau_2=\tau$ diagonal. Consequently, these values tend to be lower than other points along the transfer entropy surface, but do not have a large skew caused by false auto-transfer entropy. The largest transfer entropies are at τ_2 lags near zero because the majority of the information transfer between one response and a nearby measurement will occur at the lower

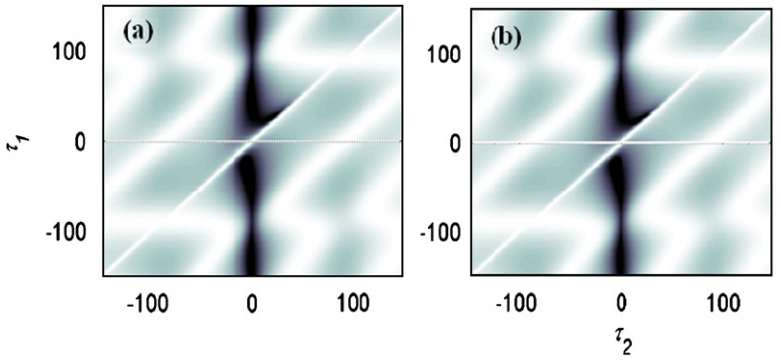

Fig. 3. Theoretical and estimated transfer entropy surfaces for (a) theoretical; $T_{x_3\to x_2}(\tau_1,\tau_2)$ and (b) estimated; $T_{x_3\to x_2}(\tau_1,\tau_2)$.

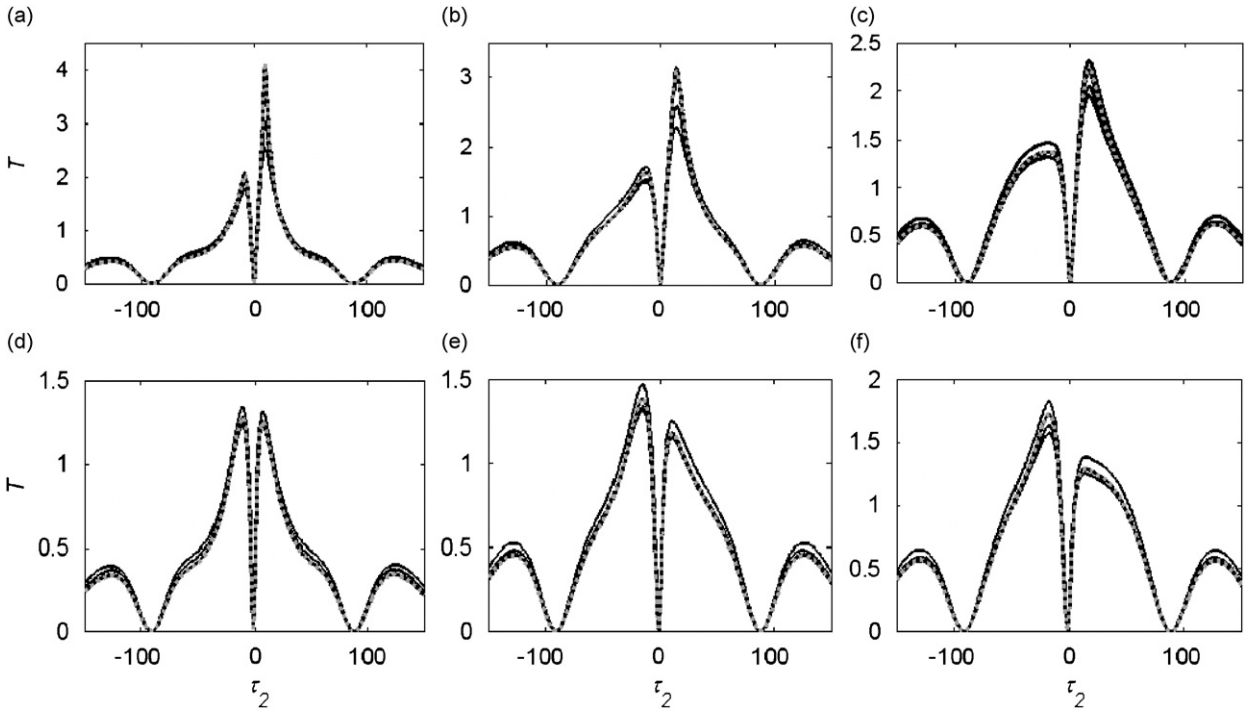

Fig. 4. Analytical and estimated transfer entropy planes (▬ estimated; ■ ■ ■ ■ theory), $T_{y\to x}(\tau_1=-1,\tau_2)$ for (a) $T_{x_1\to x_2}(\tau_1=-1,\tau_2)$, (b) $T_{x_2\to x_3}(\tau_1=-1,\tau_2)$, (c) $T_{x_3\to x_4}(\tau_1=-1,\tau_2)$, (d) $T_{x_2\to x_1}(\tau_1=-1,\tau_2)$, (e) $T_{x_3\to x_2}(\tau_1=-1,\tau_2)$, and (f) $T_{x_4\to x_3}(\tau_1=-1,\tau_2)$.

time scales before the first local minimums. When $\tau_1=0$, no transition has taken place and the transfer entropy is undefined.

Results from the estimated transfer entropy surfaces (calculated through an estimation of auto- and cross-correlations in the time series) can be compared to the purely theoretical transfer entropies in Fig. 3. As would be expected, there are very few distinctions between the two surfaces. This is true for the transfer entropies computed between any mass responses, although only one set is pictured for simplicity. Slices can be taken of the transfer entropy surface to form planes of transfer entropy in any number of directions. For the purposes of this work, the plane at $\tau_1=-1$ is examined for five of the baseline runs (Fig. 4), as this corresponds to the transfer entropy employed in previous literature [10,11] and is described in Eq. (2). Additionally, a slice was taken along the diagonal $\tau_1=\tau_2=\tau$ (Fig. 5). The estimated transfer entropy is very close to the theoretical transfer entropy along both of these sets of planes. However, the variance within the estimated transfer

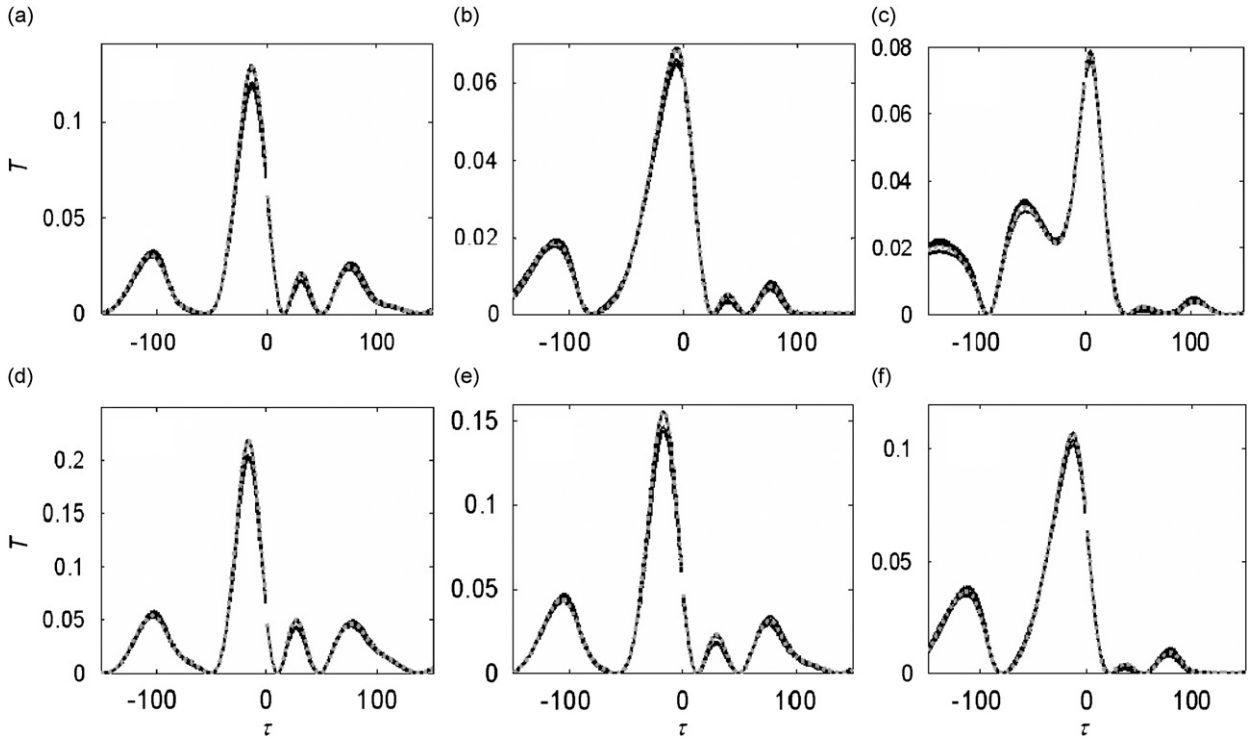

Fig. 5. Analytical and estimated transfer entropy planes (▬ estimated; ■ ■ ■ ■ theory), $T_{y\to x}(\tau_1=\tau_2=\tau)$ for (a) $T_{x_1\to x_2}(\tau_1=\tau_2=\tau)$, (b) $T_{x_2\to x_3}(\tau_1=\tau_2=\tau)$, (c) $T_{x_3\to x_4}(\tau_1=\tau_2=\tau)$, (d) $T_{x_2\to x_1}(\tau_1=\tau_2=\tau)$, (e) $T_{x_3\to x_2}(\tau_1=\tau_2=\tau)$, and (f) $T_{x_4\to x_3}(\tau_1=\tau_2=\tau)$.

entropy along the $\tau_1=\tau_2=\tau$ diagonal is slightly smaller than that along the $\tau_1=-1$ plane. For, the $\tau_1=-1$ plane, the minima are near $\tau_1\approx\pm100$ as outlined previously for the entire transfer entropy surface. There are peaks in the transfer entropy at short lags because the cross-correlation between $x(n)$ and $y(n\pm\tau_2)$ is high when τ_2 is small. However, the transfer entropy is zero at $\tau_2=-2$ because $x(n-1)$ and $y(n-2)$ are highly redundant at these delays.

Along the $\tau_1=\tau_2=\tau$ diagonal, the structure over the lags is very different. The maxima and minima are still inherently related to the auto- and cross-correlation functions, but they have a much more variable structure from one comparison to another. The larger transfer entropies are at negative delays because each mass has a greater influence on the future dynamics of adjacent masses, as would be expected for this type of structural filter. The excitation is closer to the free end, so the peak information flow from $x_{i+1}\to x_i$ is greater than the information flow from $x_i\to x_{i+1}$. The directionality of information transfer can also be noticed in the location of the peak along the delay axis. The peak in transfer entropy from $x_{i+1}\to x_i$ is at a higher negative lag than the reverse. Also, the peak is closer to the positive delays at comparisons closer to the excitation.

4. Damage identification: simulated model

As the field of structural health monitoring (SHM) has emerged, the use of system identification procedures to perform change detection [15–18] has garnered interest in the research community. Structural health monitoring involves the process of measuring and analyzing dynamic responses to structures to identify whether damage is present, as evidenced by changes in the dynamics [19]. The ability of transfer entropy to identify these types of changes will be evaluated and compared to other common change detection algorithms. To simulate a system change in the computational model, a linear stiffness reduction was introduced into each of the five originally equivalent springs k_i individually by 1, 5, 10, 25, and 50 percent for each respective damage case. Fifteen runs were simulated for the baseline condition, and five runs for each damaged

condition. The undamped natural frequencies are displayed in Fig. 6. Note that, other than for four or the 25 scenarios at 25 percent damage, the natural frequencies do not change more than 5 percent until there is a 50 percent reduction in spring stiffness.

Given linear transfer entropies estimated from the various damage cases, one can construct a damage index as in [11]. From the first ten runs at the baseline (undamaged) state, the baseline mean μ_0 and standard deviation σ_0 at each time scale can be estimated. The metric ξ for some unknown system condition is defined as

$$\xi_{y\to x}(\tau_1,\tau_2)=\frac{T_{y\to x}(\tau_1,\tau_2)-\mu_0(\tau_1,\tau_2)}{\sigma_0(\tau_1,\tau_2)}. \tag{10}$$

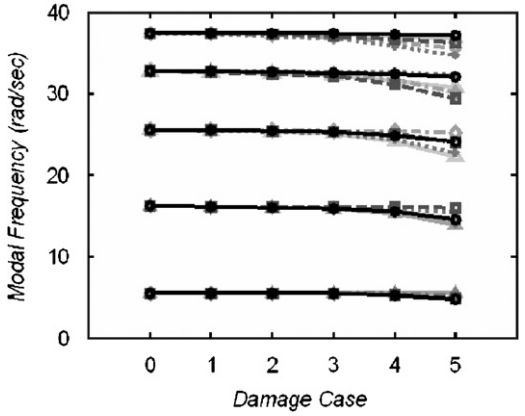

Fig. 6. Undamped resonant frequencies for each damaged spring where damage spring k_1, damage spring k_2, damage spring k_3, damage spring k_4, and damage spring k_5.

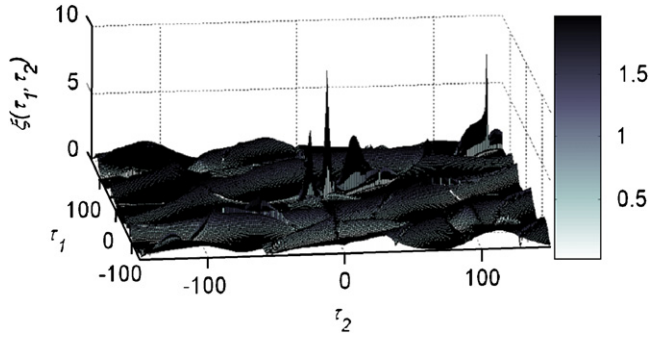

Fig. 7. $\xi_{x_2\to x_1}(\tau_1,\tau_2)$ for the transfer entropy surface with 1 percent stiffness reduction in spring k_2.

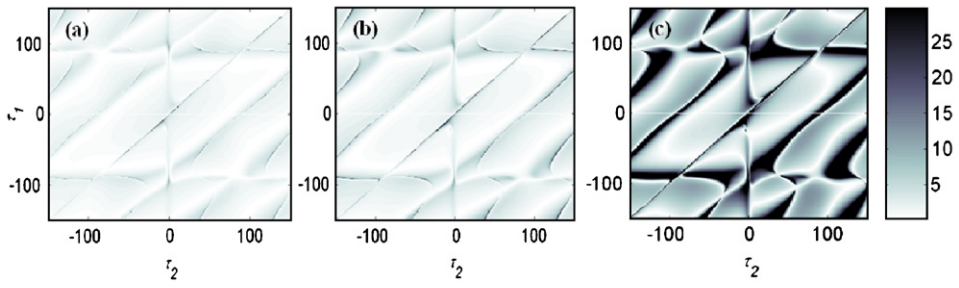

Fig. 8. $\xi_{x_2\to x_1}(\tau_1,\tau_2)$ for the transfer entropy surface with (a) 5 percent stiffness reduction in spring k_2, (b) 10 percent stiffness reduction in spring k_2, and (c) 50 percent stiffness reduction in spring k_2.

By establishing a suitable threshold for significance, the hypothesis that the system is undamaged can be tested for any set of delays in the transfer entropy surface. To reduce dimensionality of the damage index, the average normalized metric may also be formed: $\overline{\xi}_{y\to x} = 1/4\tau_1\tau_2\sum_{-\tau_1}^{\tau_1}\sum_{-\tau_2}^{\tau_2}\xi_{y\to x}(\tau_1,\tau_2)$.

Figs. 7 and 8 show damage index surfaces $\xi_{y\to x}(\tau_1,\tau_2)$ for varying degrees of damage introduced at spring k_2. It is immediately evident that the plane along the $\tau_1=\tau_2=\tau$ diagonal sees the largest increase in the damage index at the location of damage (i.e., the transfer entropy between responses on either side of the damaged spring). The sensitivity of transfer entropy along the diagonal is not unexpected because this plane does not have the false auto-transfer entropy increase brought about by the first-order Markov series assumption, as explained previously. Therefore, it may be computationally more efficient to compute the mean damage index only for delays along this diagonal, i.e., $\overline{\xi}_{y\to x} = (1/2\tau)\sum_{-\tau}^{\tau}\xi_{y\to x}(\tau,\tau)$.

As further evidence, Fig. 9 compares the diagonal-lags transfer entropy to several similar two-dimensional system identification measures for increasing damage at spring k_3. Decreasing stiffness values in spring k_3 are indicated by progressively lighter line shades, with five runs per stiffness level. Each row represents a different measure. The first row is the cross-correlation, the second row is the mutual information, third row is the transfer entropy along the $\tau_1=-1$ plane, and the fourth row is the transfer entropy along the diagonal of the transfer entropy surface. Each column represents a different location, where the measures were taken between adjacent masses around one specific spring (column 1 around k_2, column 2 around k_3, and column 3 around k_4).

The cross-correlation measurements at all three locations are nearly identical, despite differing stiffness levels, until the natural frequencies have changed significantly enough to shift the locations of maxima and minima. Another information-based feature, the time-delayed mutual information [13], shows very little change as the linear stiffness is reduced in the spring. However, there is a slightly noticeable change in the peak at $\tau=0$ at the location of damage (between responses x_3 and x_2). Similarly, transfer entropy along the $\tau_1=-1$ plane [10,11] shows a gradual difference at its peaks, however the variability in consecutive runs has increased. The last row shows the transfer entropy along the diagonal of the two-delay surface. Changes to the transfer entropy for as low as 1 percent stiffness change can be seen here, and dramatic changes are visible as the stiffness is further reduced. Note that the location of damage is immediately evident as well, as the structure of the information transfer has changed most across the responses on either side of the damaged spring. This plane of transfer entropy largely decreases for negative delays because the loss in stiffness has reduced the forward-in-time flow of information across the loosened spring.

The mean damage indices of these four two-dimensional measures (where T in Eq. (10) is replaced with the appropriate feature) plus the entire transfer entropy surface are shown in Fig. 10. Damage is introduced here in spring k_4. As in Fig. 9, increasing damage is indicated by progressively lighter shades of bars. Each location is represented by each grouping of bars along the x-axis. The value of the damage index of each measure is represented by the height of the bars. The results for each measure are displayed individually in each of the subplots (a) through (i), where (a) is the cross-correlation, (b) is the mutual information, (c) is the transfer entropy averaged over the entire transfer entropy surface, (d) is the transfer entropy averaged over the $\tau_1=-1$ plane, and (e) is the transfer entropy along the diagonal plane $\tau_1=\tau_2=\tau$.

Although the plots in Fig. 9(a)–(e) show very little differences between damage, the mean damage indices are able to extract the slight shift in natural frequencies noticeable at 25 and 50 percent stiffness loss in the spring for all but the mutual information. The results from the cross-correlation, entire transfer entropy surface, and transfer entropy along the $\tau_1=-1$ plane are fairly similar in quality. However, the damage index from the diagonal of the transfer entropy surface (Fig. 10(e)) is radically larger at the location of damage. Thus, the structural change is evident earlier, and the location of this change is immediately obvious using this feature.

These results can be further compared to common modal structural identification techniques. Fig. 11 displays results from mean damage indices composed similarly to Eq. (10) for several of these modal algorithms. Fig. 11(a) shows the mean damage index $\overline{\xi}_H$ where $\xi_{H(f)} = (H(f)-\mu_0(f))/\sigma_0(f)$, $H(f)$ is the frequency response functions of each mass response, and the mean is summed over all frequencies from 0 to 200 Hz. Additionally, Fig. 11(b) is the damage index $\xi_{f_i} = (f_i-\mu_0)/\sigma_0$ where f_i is the frequency value of each identifiable modal frequency. Note that, in the frequency response, only two of the five modal frequencies were identifiable in the simulated structure. Finally, Fig. 11(c) reveals the mean damage index $\overline{\xi}_{u_i}$, where $\xi_{u_i(n)} = (u_i(n)-\mu_0(n))/\sigma_0(n)$, $u_i(n)$ is the mode shape of each identifiable mode, and the mean is summed over

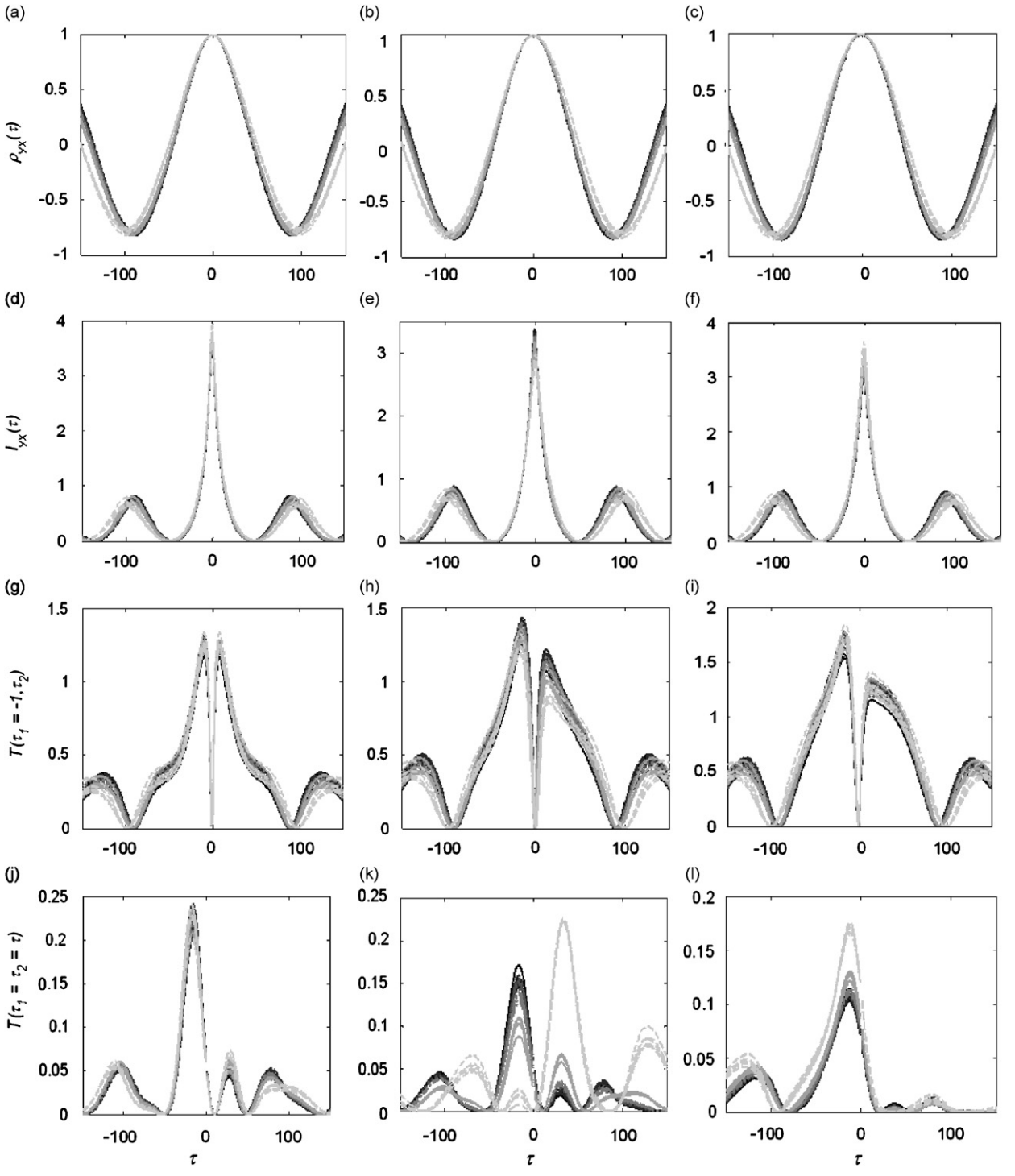

Fig. 9. Feature results for five runs at each damage condition (0, 1, 5, 10, 25, and 50 percent damage at location k_3) where (a) $\hat{R}_{x_2x_1}(\tau)$, (b) $\hat{R}_{x_3x_2}(\tau)$, (c) $\hat{R}_{x_4x_3}(\tau)$, (d) $I_{x_2x_1}(\tau)$, (e) $I_{x_3x_2}(\tau)$, (f) $I_{x_4x_3}(\tau)$, (g) $T_{x_2\to x_1}(\tau_1 = -1, \tau_2)$, (h) $T_{x_3\to x_2}(\tau_1 = -1, \tau_2)$, (i) $T_{x_4\to x_3}(\tau_1 = -1, \tau_2)$, (j) $T_{x_2\to x_1}(\tau_1 = \tau_2 = \tau)$, (k) $T_{x_3\to x_2}(\tau_1 = \tau_2 = \tau)$, and (l) $T_{x_4\to x_3}(\tau_1 = \tau_2 = \tau)$.

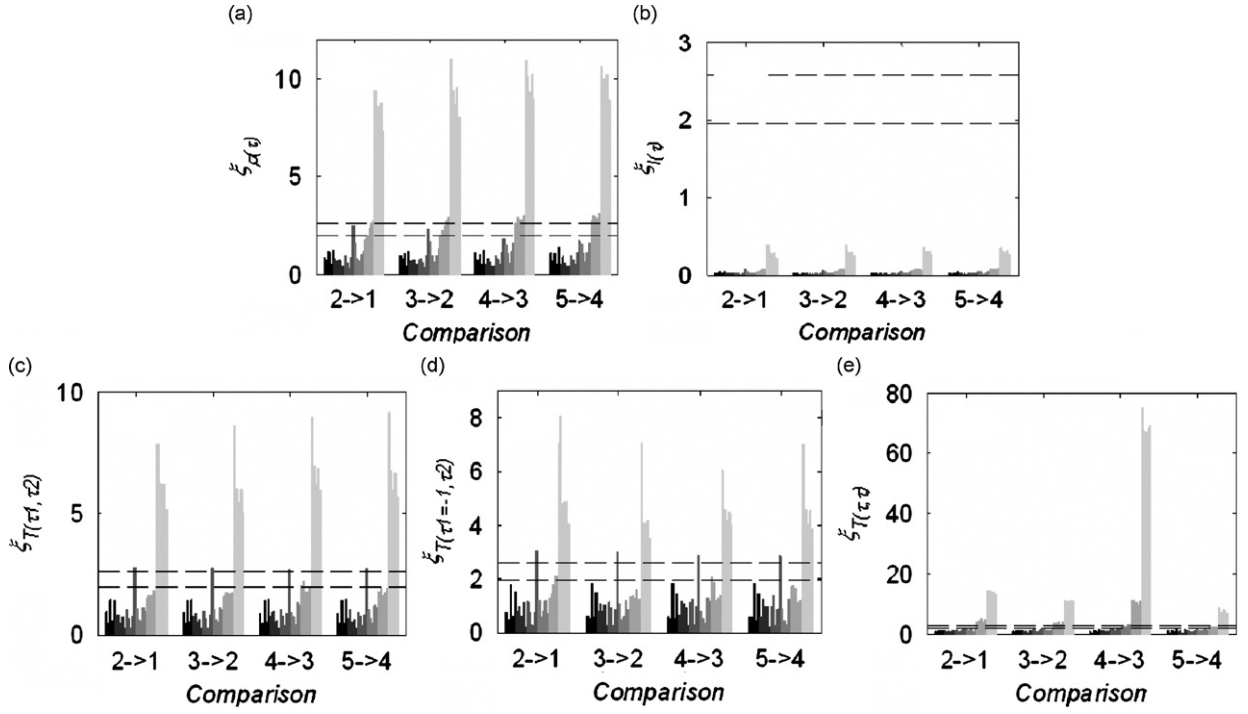

Fig. 10. Damage index ξ for five runs at each damage case (0, 1, 5, 10, 25, and 50 percent damage at location k_4), where (a) $\xi_{\hat{R}_{yx}(\tau)}$, (b) $\xi_{I_{yx}(\tau)}$, (c) $\xi_{T_{y\to x}(\tau_1,\tau_2)}$, (d) $\xi_{T_{y\to x}(\tau_1=-1,\tau_2)}$, and (e) $\xi_{T_{y\to x}(\tau_1=\tau_2=\tau)}$. The dotted lines represent the 95 (lower line) and 99 percent (higher line) confidence levels assuming a Gaussian response.

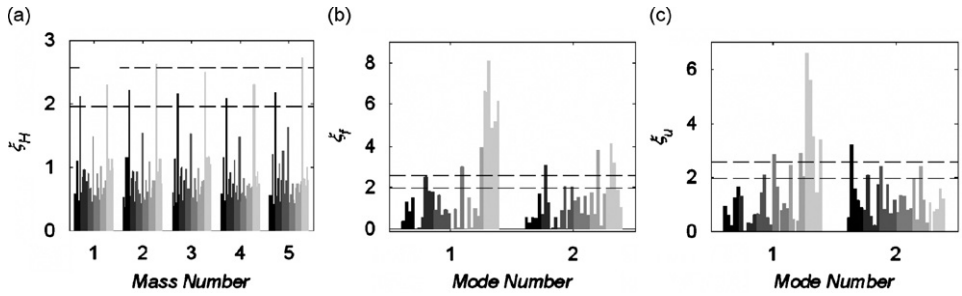

Fig. 11. Damage index ξ for five runs at each damage case (0, 1, 5, 10, 25, and 50 percent damage at location k_4), where (a) ξ_H, (b) ξ_{f_i}, and (c) ξ_{u_i}. The dotted lines represent the 95 (lower line) and 99 percent (higher line) confidence levels assuming a Gaussian response.

all nodes from x_1 to x_5. The modal frequencies and mode shapes were determined using the frequency-based rational polynomial curve fitting algorithm [1] and the software found in [20]. Examining direct changes to the frequency response functions, one is not able to predict the onset of structural changes at all within the range of damage simulated. The first modal frequency and mode shape is able to identify a 50 percent stiffness change in the fourth spring, but this metric is not as sensitive as most of the time-based measures from Fig. 10. For this computational example, the modified transfer entropy introduced in this work is much more sensitive to the simulated changes than any of the other techniques compared.

Assuming the response in each run is Gaussian, and the system is nominally linear, the damage index can be compared to a confidence limit based on a standard normal distribution. The thresholds, $S = 1.96$ and 2.5758 for 95 and 99 percent confidence are shown as dashed lines in Figs. 10 and 11. To incorporate the confidence

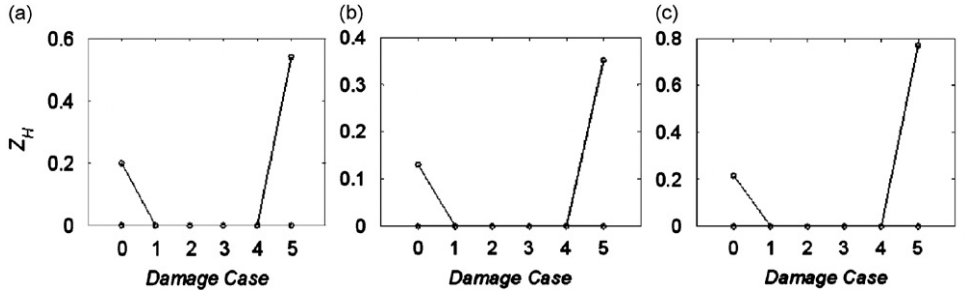

Fig. 12. Damage index Z_H for five runs at each damage case (damage in fourth spring, k_4); (a) x_3, (b) x_4, and (c) x_5.

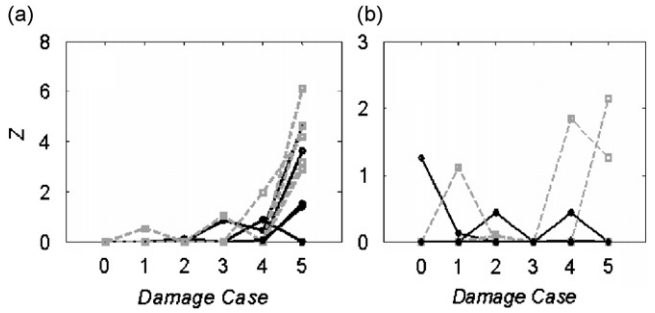

Fig. 13. Damage index Z for five runs at each damage case (damage in fourth spring, k_4), where Z_{f_i} and Z_{u_i}; (a) mode number 1 and (b) mode number 2.

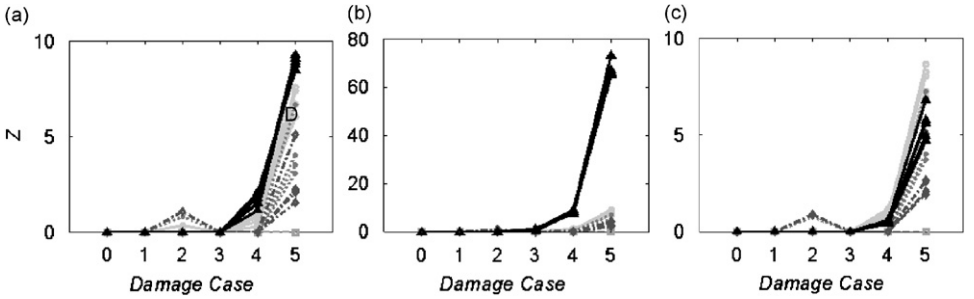

Fig. 14. Damage index Z for five runs at each damage case (damage in fourth spring, k_4) where $Z_{\hat{R}_{yx}(\tau)}$, $Z_{I_{yx}(\tau)}$, $Z_{T_{y\to x}(\tau_1,\tau_2)}$, $Z_{T_{y\to x}(\tau_1=-1,\tau_2)}$, and damage $Z_{T_{y\to x}(\tau_1=\tau_2=\tau)}$; (a) $x_3 \to x_2$, (b) $x_4 \to x_3$, and (c) $x_5 \to x_4$.

level, a final damage index Z can be introduced such that non-zero values appear only above the set threshold:

$$Z = (\overline{\xi} - S)\Theta(\overline{\xi} - S), \tag{11}$$

where Θ is the unit step function. Thus, a positive Z indicates that the hypothesis the system is undamaged is rejected with some confidence. The Z results for the spring k_4 damage scenario are shown for each of the compared features in Figs. 12–14. As evident in the formerly displayed bar chart results, the transfer entropy along the diagonal of the two-lag surface is most sensitive to any changes in stiffness in the spring. At response locations other than the location of damage, this modification of the transfer entropy is able to capture differences caused by damage as well or better than each of the other features considered. At the specific location of damage, the modified transfer entropy is quite superior, with as much as eight times higher values in its damage index Z.

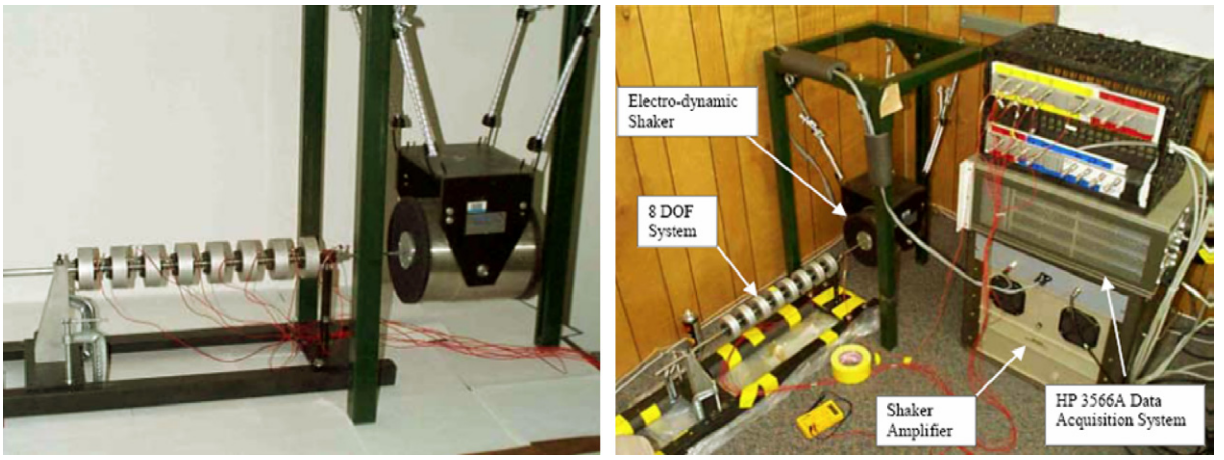

Fig. 15. Experimental setup.

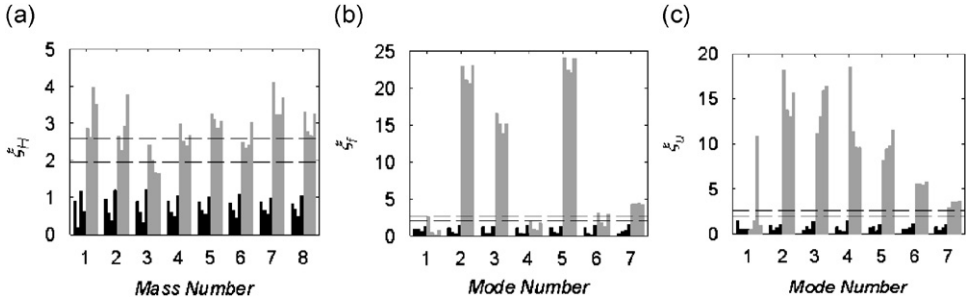

Fig. 16. Damage index ξ for four runs per scenario (undamaged, 14 percent damage at fifth spring), where (a) ξ_H, (b) ξ_{f_i}, and (c) ξ_{u_i}. The dotted lines represent the 95 percent (lower line) and 99 percent (higher line) confidence levels assuming a Gaussian response.

5. Damage identification: experimental structure

To further corroborate the results evidenced in the simulated oscillator, an experimental multi-degrees-of-freedom oscillator was analyzed (Fig. 15). The experimental setup and data collection was performed at the Los Alamos National Laboratory, Engineering Institute for Structural Health Monitoring, Damage Prognosis, and Validated Simulations, the data of which can be obtained from their website (http://www.lanl.gov/projects/ei/). The system is assembled from eight translating masses connected by springs. Each mass is a 25.4 mm thick, 76.2 mm diameter aluminum disc. A highly-polished steel rod slides through a hole in the center of each disc to support the masses vertically while constraining them to horizontal motion only. The mass holes are lined with a Teflon bushing and affixed to small steel collars with bolts. The springs between each mass are epoxied to the steel collars.

A Hewlett-Packard 3566A data acquisition system was used, consisting of a 35650 mainframe, 35653A source module, four 35653A 8-channel input modules, and a 35651C signal processing module. A PCB type 204 force transducer is present at the connection to the 215-N peak force electro-dynamic shaker. An Endevco type 2251A-10 accelerometer is bonded to each mass element. The masses are labeled sequentially with the first located at the end attached to the shaker. Each degree of freedom has a mass of 419.4 g except for the first, which has a mass of 559.3 g because of the hardware needed to attach the shaker.

The undamaged condition consists of identical springs with a linear spring constant of 56.7 kN/m. For the damaged condition, the fifth spring counting from the shaker end was replaced by a spring with a linear spring constant of 49.0 kN/m (a 14 percent reduction in stiffness). Four runs at 3, 4, 5, and 6 V, respectively were applied for both the undamaged and damaged conditions. Data was sampled at 500 Hz for 8 s for each run. All damage indices were computed as in Eqs. (10) and (11).

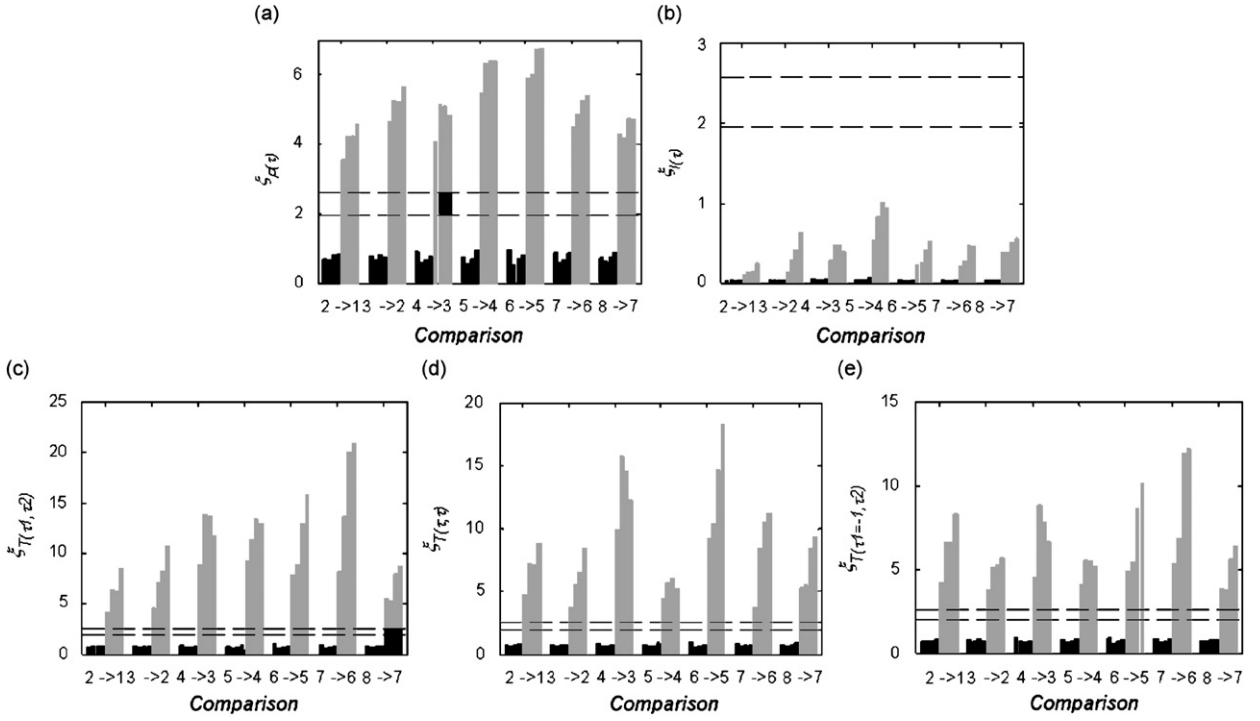

Fig. 17. Damage index ξ for four runs per scenario (undamaged, 14 percent damage at fifth spring) where (a) $\xi_{\dot{R}_{yx}(\tau)}$, (b) $\xi_{I_{yx}(\tau)}$, (c) $\xi_{T_{y\to x}(\tau_1,\tau_2)}$, (d) $\xi_{T_{y\to x}(\tau_1=-1,\tau_2)}$, and (e) $\xi_{T_{y\to x}(\tau_1=\tau_2=\tau)}$. The dotted lines represent the 95 percent (lower line) and 99 percent (higher line) confidence levels assuming a Gaussian response.

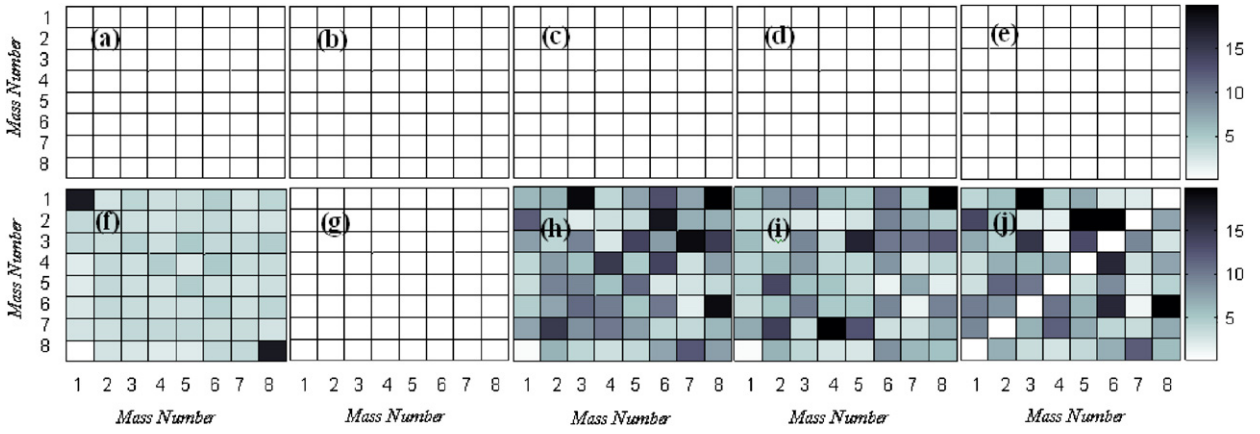

Fig. 18. Damage Index Z for the experimental oscillator for (a) undamaged; $\rho_{xy}(\tau)$, (b) undamaged; $I_{xy}(\tau)$, (c) undamaged; $T_{y\to x}(\tau_1=-1,\tau_2)$, (d) undamaged; $T_{y\to x}(\tau_1=\tau_2=\tau)$, (e) undamaged; $T_{y\to x}(\tau_1,\tau_2)$, (f) 14 percent damage in fifth spring; $\rho_{xy}(\tau)$, (g) 14 percent damage in fifth spring; $I_{xy}(\tau)$, (h) 14 percent damage in fifth spring; $T_{y\to x}(\tau_1,\tau_2)$, (i) 14 percent damage in 5th spring;$T_{y\to x}(\tau_1=-1,\tau_2)$, and (j) 14 percent damage in fifth spring; $T_{y\to x}(\tau_1=\tau_2=\tau)$.

Damage index ξ results from each system identification technique can be viewed in Figs. 16 and 17. The frequency response functions are properly able to characterize the presence of a linear system change. Seven modes were identifiable from the frequency response functions. Four of these modes showed significant changes to their peak frequencies, while six mode shapes conveyed such differences. From the time-domain based measures (Fig. 17), only the mutual information is unable to see the structural stiffness change at each of the response comparisons. The transfer entropy-based damage indices show more drastic increases to the damage

index than the cross-correlation. The modified transfer entropy surface and diagonal damage indices have slightly higher values than the previously employed transfer entropy along the $\tau_1 = -1$ plane. Also, only the cross-correlation and transfer entropy along the diagonal have maximum damage indices at the correct location of damage. For each of the time-domain based measures, the damage index Z is plotted for each of the possible response comparisons for one representative run (Fig. 18). It is evident that the modified transfer entropy surface and transfer entropy plane along the diagonal are both more sensitive and better able to locate damage.

Although transfer entropy appears to be equal to if not superior to all other system identification techniques compared, the dramatic differences in location-specific sensitivity in the modified diagonal transfer entropy are less obvious in this experiment than in the simulated model. The decreased sensitivity in the experimental results is most likely attributable to changes in boundary conditions between the undamaged and damaged results. In order to change the stiffness in the interior spring as required for the damage condition in this experiment, connections between elements in the structure must be taken apart and reattached. Consequently, a more global boundary condition change is noticeable in the responses. The more locally dependent modified transfer entropy along the diagonal is able to detect the change as well as or better than the other metrics, similar to the computational model at comparisons at other damage locations (Figs. 14(a) and (c)). However, the local differences in information exchange are not much more noticeable at the comparisons at the specific location of damage itself, as was the case in the computational model. A different experiment that allows the practitioner to change the stiffness linearly at one location without requiring these boundary condition changes between elements in the structure may be better suited for seeing the expected dramatic local changes in the modified transfer entropy along the diagonal time delays.

6. Summary and discussion

An expansion of the transfer entropy was developed that incorporates two time delays to form a transfer entropy surface. This modification examines additional time scales of the information flow not present in previously proposed applications of transfer entropy for system identification. The entire surface or some subset of the surface can be analyzed. Previous literature utilizing the transfer entropy used a time delay such that lags in only one of the processes under consideration were examined. The use of two lags allows for additional interpretations of the influences between various processes at further time scales without the computational burden and variability introduced through higher order Markov models. Theoretical values for this transfer entropy surface were derived and compared favorably to estimated values assuming a linear structural dynamics model. From a structural damage detection perspective, using the diagonal set of time lags from this newly introduced transfer entropy surface provides greater sensitivity to damage, as well as a capability for damage localization not previously attainable with other forms of the transfer entropy.

Specifically, the transfer entropy was examined in its ability to determine the onset of linear stiffness changes to computational and experimental multi-degrees-of-freedom oscillators subject to random Gaussian excitation. Damage indices formed from the transfer entropy surface were compared with several other common system identification techniques, including cross-correlations, frequency response functions, modal frequencies, mode shapes, and mutual information. For the provided examples, the diagonal of the transfer entropy surface was validated to have as good or better sensitivity to structural changes than all other metrics compared. The modified transfer entropy along the diagonal is superior in its ability to locate damage in the structure as well.

Interestingly, the estimation of transfer entropy (assuming a linear model) is actually made using auto- and cross-correlations, yet the sensitivity to damage and damage location for certain time lags in the transfer entropy is much higher than the auto- or cross-correlation alone. The transfer entropy is a complicated nonlinear function of several auto- and cross-correlations, and this particular combination results in much greater changes in the presence of damage. Specific components of various auto- and cross-correlations are emphasized or de-emphasized by the expression such that damage-specific (stiffness) changes to the system are more noticeable at the location of damage. Transfer entropy in this work is formulated in such a way as to describe the (possibly bi-directional) flow of information between locations on a structure, while still being grounded in a functional relationship with more widely understood concepts such as auto- and cross-correlations. This formulation and relationship results in a measure more locally sensitive to damage than other common linear system identification measures.

Each technique was constructed based on a model assuming Gaussian forcing and no higher than second-order correlations in the data. If one were interested in model-unspecific or nonlinear system changes, then the transfer entropy features can still be utilized if probabilities in the transfer entropy expression are estimated directly rather than under the linear model assumption. These estimations can be difficult, and therefore, if the linear assumption can be made, the technique introduced in this work is advisable. However, many forms of structural damage can manifest as the presence of nonlinearity, e.g., opening and closing of a crack or loss in preload in a bolted connection. Future work will attempt to perform a complete estimation of the modified transfer entropy introduced here for the purposes of generalized system change identification and nonlinearity detection, possibly using tailored surrogates.

Acknowledgments

The first author acknowledges support through a National Science Foundation Graduate Research Fellowship. This work was performed under the auspices of the UCSD/Los Alamos National Laboratory Engineering Institute for Structural Health Monitoring, Damage Prognosis, and Validated Simulations (Contract #72232-001-04 43), with specific thanks to the Institute for the free DIAMOND experimental modal analysis software and for providing the experimental data on their web page (http://www.lanl.gov/projects/ei/).

References

[1] M.H. Richardson, D.L. Formenti, Parameter estimation from frequency response measurements using rational fraction polynomials, Structural Measurement Systems Technical Note 85-3, 1985.
[2] G.H. McVerry, Structural identification from the frequency domain from earthquake records, *Earthquake Engineering and Structural Dynamics* 8 (1980) 161–180.
[3] J.N. Juang, R.S. Pappa, An eigensystem realization algorithm for modal parameter identification and model reduction, *Journal of Guidance, Control and Dynamics* 8 (1985) 620–627.
[4] H. Vold, J. Kundrat, T. Rocklin, R. Russel, A multi-input modal estimation algorithm for mini-computers, *SAE Transactions* 91 (1985) 815–821.
[5] S. Fahey, J. Pratt, Time domain modal estimation techniques, *Experimental Techniques* 22 (1998) 45–49.
[6] K.A. Petsounis, S.D. Fassois, Parametric time-domain models for the identification of vibrating structures—a critical comparison and assessment, *Mechanical Systems and Signal Processing* 15 (2001) 1031–1060.
[7] D.E. Adams, Frequency domain ARX model and multi-harmonic FRF estimators for non-linear dynamic systems, *Journal of Sound and Vibration* 250 (2002) 935–950.
[8] K. Worden, G.R. Tomlinson, Nonlinearity in experimental modal analysis, *Philosophical Transactions of the Royal Society A* 259 (2001) 113–130.
[9] T. Schreiber, Measuring information transfer, *Physical Review Letters* 85 (2000) 461–464.
[10] J.M. Nichols, Examining structural dynamics using information flow, *Probabilistic Engineering Mechanics* 21 (2006) 420–433.
[11] J.M. Nichols, M. Seaver, S.T. Trickey, M.D. Todd, C.C. Olson, L.A. Overbey, Detecting nonlinearity in structural systems using the transfer entropy, *Physical Review E* 72 (2005) 1–11.
[12] T.M. Cover, J.A. Thomas, *Elements of Information Theory*, Wiley, New York, 1991.
[13] J.A. Vastano, H.L. Swinney, Information transport in spatiotemporal systems, *Physical Review Letters* 85 (1988) 461.
[14] A. Kaiser, T. Schreiber, Information transfer in continuous processes, *Physica D* 166 (2002) 43–62.
[15] R.P. Sampaio, N.M.M. Maia, J.M.M. Silva, Damage detection using the frequency-response-function curvature method, *Journal of Sound and Vibration* 226 (1999) 1029–1042.
[16] N. Stubbs, C. Sikorsky, S.C. Park, R. Bolton, Verification of a methodology to nondestructively evaluate the structural properties of bridges, *Proceedings of the Second International Workshop on Structural Health Monitoring*, Stanford University, Palo Alto, CA, USA, September 1999.
[17] H. Sohn, K.H. Law, Extraction of Ritz vectors and application to structural damage diagnosis, in: *The Fifth US National Congress on Computational Mechanics*, Boulder, Colorado, 1999.
[18] M.A. Norris, L. Meirovitch, On the problem of modeling for parameter identification in distributed structures, *International Journal for Numerical Methods in Engineering* 28 (1989) 2451–2463.
[19] S.W. Doebling, C.R. Farrar, M.B. Prime, A summary review of vibration-based damage identification methods, *Shock and Vibration Digest* 205 (1998) 631–645.
[20] S.W. Doeblin, C.R. Farrar, P.J. Cornwell, DIAMOND: a graphical user interface toolbox for comparative modal analysis and damage identification, *Proceedings of the Sixth International Conference on Recent Advances in Structural Dynamics*, Southampton, July 1997.